

# Measuring Type Ia Supernova Distances and Redshifts From Their Multi-band Light Curves

Alex G. Kim<sup>a</sup> Ramon Miquel<sup>b</sup>

<sup>a</sup>*Physics Division, Lawrence Berkeley National Laboratory, Berkeley, CA 94720, USA*

<sup>b</sup>*Institució Catalana de Recerca i Estudis Avançats (ICREA)  
Institut de Física d'Altes Energies (IFAE)  
Edifici Cn, Campus UAB, E-08193 Bellaterra (Barcelona), Spain*

---

## Abstract

The distance and redshift of a type Ia supernova can be determined simultaneously through its multi-band light curves. This fact may be used for imaging surveys that discover and obtain photometry for large numbers of supernovae; so many that it would be difficult to obtain a spectroscopic redshift for each. Using available supernova-analysis tools we find that there are several conditions in which a viable distance–redshift can be determined. Uncertainties in the effective distance at  $z \sim 0.3$  are dominated by redshift uncertainties coupled with the steepness of the Hubble law. By  $z \sim 0.5$  the Hubble law flattens out and distance-modulus uncertainties dominate. Observations that give  $S/N = 50$  at peak brightness and a four-day observer cadence in each of *griz*-bands are necessary to match the intrinsic supernova magnitude dispersion out to  $z = 1.0$ . Lower  $S/N$  can be tolerated with the addition of redshift priors (e.g. from a host-galaxy photometric redshift), observations in an additional redder band, or by focusing on supernova redshifts that have particular leverage for this measurement. More stringent  $S/N$  requirements are anticipated as improved systematics control over intrinsic color, metallicity, and dust is attempted to be drawn from light curves.

*Key words:* cosmology:distance scale, supernovae:general

---

## 1 Introduction

Proposed wide-field imaging surveys will be able to discover and build light curves of thousands to hundreds of thousands of high-redshift type Ia supernovae (SNe Ia). SNe Ia are established as excellent distance indicators having

been used for both for the measurement of the Hubble Constant [1] and for the discovery of the accelerated expansion of the Universe [2,3]. There is thus interest in exploring how supernovae in new surveys can be used to improve the measurement of the expansion history of the Universe and provide further insight into the physical cause of its acceleration.

Although planned facilities and surveys provide straightforward harvesting of light curves for large numbers of supernovae, the corresponding spectroscopic observations used for redshift determination, supernova typing, and diagnostics are expensive. It is unclear whether there will be available spectroscopic resources commensurate to the production of the imaging. In addition, those surveys that target spectroscopy for a specific redshift range will still accumulate supernova light curves at other redshifts [4]. There is therefore interest in the possibility of performing supernova cosmology analysis with photometric data only. In this scenario, light curves not only fill their traditional role in measuring distances but are also responsible for supernova typing and redshift determination.

In this paper, we explore the feasibility of using survey photometry to simultaneously estimate distance and redshift using fits to a light-curve template. We do not incorporate typing and assume that the supernova is already known to be type Ia. We use an effective distance-modulus uncertainty as the metric of interest. Barris and Tonry [5] describe an alternative approach to the same problem using Bayesian statistics and marginalizing over redshift, obtaining distance precisions close to the intrinsic corrected SN Ia magnitude dispersion. Other papers have considered other combinations of information derivable from photometric data only: Johnson and Crofts [6] and Kuznetsova and Connolly [7] for photometric supernova typing; Sullivan et al. [8] for simultaneous typing and redshift determination with early light curves; and Wang [9] for supernova photometric redshifts. The effect of supernova redshift uncertainties on the determination of dark-energy parameters is examined in Huterer et al. [10].

This paper is organized as follows: §2 describes our approach towards estimating distance modulus and redshift uncertainties for photometric survey data through light curve fitting. In §3 we specify the properties of the six surveys that we consider: all share a four-day cadence but have differing depths that correspond to obtaining a signal-to-noise (S/N) of either 25 or 50 for a fiducial  $z = 0.325, 0.731, \text{ or } 1.11$  supernova at peak brightness in each band. Interesting features of our results are discussed in §4 and conclusions are presented in §5.

## 2 Approach

Our objective is to determine how well the distance and redshift of a single supernova can be determined from a set of photometric data. We use a parameterized description of the time-evolving spectral energy distributions (SEDs) for SNe Ia incident to the observer. An individual supernova is characterized by the date of explosion and redshift in addition to the parameters of the SED model. The survey is described by the observing cadence, photometric noise, and bands of observation. Model-parameter uncertainties from light-curve fitting are estimated using the Fisher information matrix. These parameters are in turn propagated into a covariance matrix for the distance modulus and redshift. The covariance matrix is distilled into an effective distance modulus uncertainty to aid in the interpretation of the results. The Fisher analysis provides a firm lower limit on the errors one can obtain: this limit is an excellent estimate of errors when the data uncertainties are small and Gaussian distributed.

SALT2 [11] provides an empirical model for the time evolving SED of SNe Ia. The model is constructed from a training set of spectroscopic and photometric measurements of both low- and high-redshift supernovae. SALT2 models the SED as a function of phase  $p$  and wavelength  $\lambda$  by

$$N_{\ln\lambda}(p, \lambda; x_0, x_1, c) = x_0 \times [M_0(p, \lambda) + x_1 M_1(p, \lambda)] \times e^{cCL(\lambda)} \quad (1)$$

where the model parameters  $x_0$ ,  $x_1$ , and  $c$  correspond (approximately) to the peak luminosity, light-curve shape, and observed color. The color parameterization simultaneously accounts for intrinsic supernova color variation and foreground dust extinction. The functions  $M_0$ ,  $M_1$ , and  $CL$  are constructed according to the training set. The model covers supernova phases from  $[-20, +50]$  days and the wavelength range  $[2000, 9200]$  Å. We work with photon rather than energy fluxes since they, combined with transmission functions, describe counter detectors and observer magnitude systems [12]. The use of densities in  $\ln \lambda$  rather than  $\lambda$  simplifies the description of redshifted spectra.

The residual dispersion of the training set data from the model gives a quantitative estimate of how well SALT2 represents supernovae. SALT2 treats the dispersion of the template light curves of an average  $x_1=0$ ,  $c = 0$  supernova as

$$\sigma_{disp}(N(p, \lambda)) = N(p, \lambda) \sqrt{V0(p, \lambda)} DS(p, \lambda) \quad (2)$$

where  $\lambda$  is the effective wavelength of the band in the SN-frame and the functions for variance,  $V0$ , and dispersion scaling,  $DS$ , are provided with the software distribution<sup>1</sup>. Correlations between the residuals within a light curve,

---

<sup>1</sup> <http://supernovae.in2p3.fr/~guy/salt/index.html>

though non-zero, are not quantified. Dispersion in colors are given [11] by a wavelength-dependent, phase-independent magnitude dispersion

$$\sigma_{col}(\lambda) = \begin{cases} 0.022 \left( \frac{\lambda - \lambda_B}{\lambda_U - \lambda_B} \right)^3 & \text{if } \lambda < \lambda_B, \\ 0.018 \left( \frac{\lambda - \lambda_V}{\lambda_R - \lambda_V} \right)^2 & \text{if } \lambda > \lambda_V, \\ 0 & \text{if } \lambda_B \leq \lambda \leq \lambda_V. \end{cases} \quad (3)$$

The survey data are described by the band of observation and photometric uncertainty. Each supernova is observed with an undisrupted cadence in all bands. Observations are tuned to provide a fixed signal-to-noise at peak brightness in each band for an average  $x_1 = 0$ ,  $c = 0$  supernova, and assume a sky dominated background for calculating the noise off-peak. This noise model approximately describes data from a ground-based rolling supernova search (e.g. Astier et al. [13]).

The supernova light curves are modeled using the SALT2 SED model with the addition of parameters for the date of explosion  $t_0$  and redshift  $z$

$$f(t, X; \mathbf{p}) = \int T_X(\lambda) N_{\ln \lambda} \left( \frac{t}{1+z} - t_0, \frac{\lambda}{1+z}; x_0, x_1, c \right) d \ln \lambda \quad (4)$$

where  $T_X$  is the transmission of band  $X$ . The complete parameter set for the light-curve model is  $\mathbf{p} = \{t_0, z, x_0, x_1, c\}$ .

Parameter uncertainties from light-curve fitting are determined through the Fisher information matrix  $\mathbf{F}$  [14]. Every data point in all useful bands are included in the calculation. Note that for the surveys we consider, photometric noise is independent of the light-curve parameters. Any independent redshift prior uncertainties are added to the  $F_{zz}$  element. The covariance matrix of the parameters is the inverse of the Fisher matrix  $\mathbf{F}^{-1}$ .

In SALT2, light-curve parameters are used to calculate the distance modulus through the relation

$$\mu = -2.5 \log(x_0) + \alpha_x \times x_1 - \beta \times c + \text{const} \quad (5)$$

with  $\alpha = 0.13$  and  $\beta = 1.77$ . The covariance matrix  $\mathbf{U}$  of the parameters  $\boldsymbol{\eta} = \{\mu, z\}$  is given by

$$U_{ij} = \sum_{k,l} \frac{\partial \eta_i}{\partial p_k} \frac{\partial \eta_j}{\partial p_l} (\mathbf{F}^{-1})_{kl}. \quad (6)$$

Cosmological parameter fitting can proceed with the likelihood function dependent on the  $\mu - z$  covariance matrix for each supernova. However, to avoid

analysis of this non-Gaussian likelihood and provide intuitive insight, we consider the limiting case where redshift uncertainties are small. Taylor expanding the theoretical prediction of the distance modulus  $\mu_\gamma$  around the observed redshift, the probability distribution function to first order is Gaussian with a  $\chi^2$  for the one parameter  $\mu$  with an effective variance

$$(\sigma_{\mu,eff})^2 = U_{\mu\mu} + \left(\frac{d\mu_\gamma}{dz}\right)^2 U_{zz} + 2\frac{d\mu_\gamma}{dz}U_{\mu z}. \quad (7)$$

(See §A for a sketch of the derivation.) In this fashion, uncertainties in  $z$  and their correlation with  $\mu$  are incorporated into an effective uncertainty in distance modulus. We use the distance modulus for a photon-counting magnitude system that is related to the standard distance modulus by  $\mu_\gamma = \mu - 2.5 \log(1+z)$ . As  $d\mu_\gamma(z)/dz > 0$  for most all cosmologies of interest, positive correlations in  $\mu$  and  $z$  increase the effective distance modulus uncertainty.

### 3 SN Model and Survey Specification and Results

We adopt a baseline description of SALT2 and the supernova survey. The covariance matrix of the SALT2 templates between points  $i$  and  $j$  (with phases  $p_i$  and  $p_j$  observed in bands  $X_i$  and  $X_j$ ) is based on the residuals given by Equations 2 and 3:

$$V_{ij} = \begin{cases} \sigma_{i,disp}\sigma_{j,disp}\text{sinc}\left(\pi\frac{p_i-p_j}{5\text{ days}}\right) + \sigma_{i,col}\sigma_{j,col} & \text{if } X_i = X_j, \\ 0 & \text{if } X_i \neq X_j. \end{cases} \quad (8)$$

We have modeled the day-to-day correlations in the residuals with the  $\text{sinc}(x) = \sin x/x$  function with a time scale of 5 days; this keeps the intrinsic light curves smooth and provides both positive and negative correlations. Residuals in different bands are uncorrelated. Operationally, this covariance matrix of the model dispersion is added to that of the photometric data.

We consider only data at supernova phases covered by the SALT2 model; observations around peak brightness provide most of the leverage in light-curve fits with our sky-limited background.

Observations are modeled as being made in the Megacam *griz*-bands of the Canada-France-Hawaii Telescope with the transmissions provided with the SALT2 software distribution.

As SALT2 is not well trained at wavelengths smaller than the  $U$ -band and as SNe Ia have little emission at these low wavelengths, we do not use observations in this regime. This naturally defines three specific redshifts to consider,

Table 1

Supernova-frame effective wavelengths in microns for observer *griz*-bands. The three redshifts in the table correspond, respectively, to matches of observer *gri* to the restframe *U*.

redshift	<i>g</i>	<i>r</i>	<i>i</i>	<i>z</i>
0.325	0.36	0.47	0.58	0.69
0.731	0.28	0.36	0.44	0.53
1.118	0.23	0.29	0.36	0.43

Table 2

$\mu$ - $z$  covariance and effective  $\mu$  uncertainties: Peak  $S/N = 25$ , four-day cadence

$z_{SN}$	$\sigma_{prior}(z) = \text{none}$		$\sigma_{prior}(z) = 0.01$		$\sigma_{prior}(z) = 10^{-3}$	
	<b>U</b>	$\sigma_{\mu,eff}$	<b>U</b>	$\sigma_{\mu,eff}$	<b>U</b>	$\sigma_{\mu,eff}$
0.32	$\begin{pmatrix} 0.0021 & 3.8E-4 \\ 3.8E-4 & 2.5E-4 \end{pmatrix}$	0.14	$\begin{pmatrix} 0.0017 & 1.1E-4 \\ 1.1E-4 & 7.1E-5 \end{pmatrix}$	0.082	$\begin{pmatrix} 0.0015 & 1.6E-6 \\ 1.6E-6 & 1.0E-6 \end{pmatrix}$	0.040
0.731	$\begin{pmatrix} 0.0023 & 2.0E-4 \\ 2.0E-4 & 8.5E-5 \end{pmatrix}$	0.065	$\begin{pmatrix} 0.0021 & 1.1E-4 \\ 1.1E-4 & 4.6E-5 \end{pmatrix}$	0.056	$\begin{pmatrix} 0.0018 & 2.3E-6 \\ 2.3E-6 & 9.9E-7 \end{pmatrix}$	0.043
1.118	$\begin{pmatrix} 0.10 & 0.012 \\ 0.012 & 0.0016 \end{pmatrix}$	0.39	$\begin{pmatrix} 0.017 & 7.0E-4 \\ 7.0E-4 & 9.4E-5 \end{pmatrix}$	0.14	$\begin{pmatrix} 0.012 & 7.5E-6 \\ 7.5E-6 & 1.0E-6 \end{pmatrix}$	0.11

$z = \{0.325, 0.731, 1.118\}$ , where the effective wavelengths of the *gri*-bands in turn match that of the SN-frame *U*. The SN-frame wavelengths that correspond to each observer band are given in Table 1. The number of data points for each supernova is  $\frac{70 \text{ days}}{\text{cadence}}(1+z)N_{bands}$ . At  $z = 0.325$  there are a total 92 data points in *griz*-bands used in the analysis. At  $z = 0.731$  there are 90 points in *riz*-bands and at  $z = 1.118$  74 points in *iz*-bands. When the *z*-band observes the SN *U*, there is no second band for a color measurement and the fit is not constrained.

The partial derivatives of the data model of Equation 4 with respect to its parameters are shown for the three redshifts in Figures 1, 2, and 3.

We consider surveys designed to provide signal-to-noise of either 25 or 50 for a single visit at the peak brightness of each band for an average  $x_1 = 0$ ,  $c = 0$  supernovae at these specific redshifts. Each band is observed with a four-day observing cadence. To simulate the range of possible spectroscopic or host-galaxy photometric redshifts, we include redshift priors with precisions of  $10^{-3}$ , 0.01, as well as the case of no prior; we expect that supernova photometric redshifts will easily exclude the extreme non-Gaussian tails from galactic photometric redshifts. We use a flat  $\Lambda$  universe with  $\Omega_M = 0.3$  to get  $d\mu_\gamma/dz$  (used in Equation 7) of 6.9, 3.1, and 1.9 for the three redshifts. The resulting  $\mu$ - $z$  covariance matrices and effective  $\mu$  uncertainties are given in Table 2 for  $S/N = 25$  and Table 3 for  $S/N = 50$ . Although the results are grouped according to the  $S/N$  at peak brightness, the surveys that generate these data are different for each redshift: the survey that corresponds to the high-redshift supernova is deep and obtains higher  $S/N$  for supernovae at lower redshift.

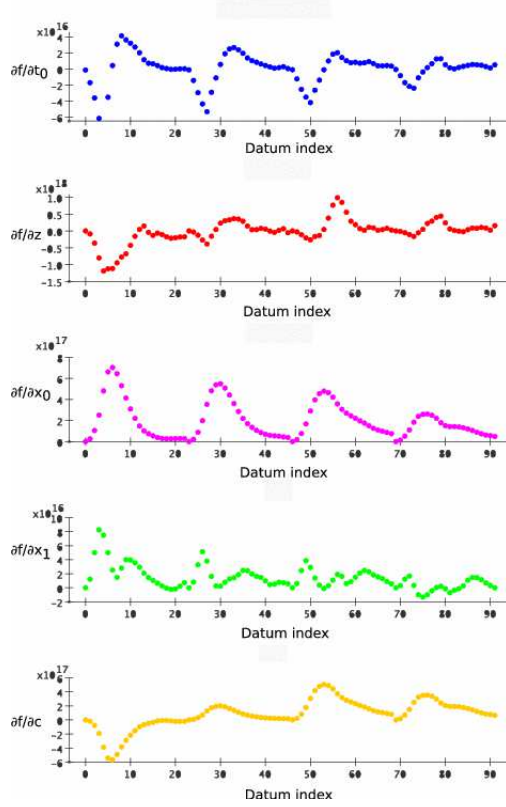


Fig. 1.  $\partial f/\partial \mathbf{p}$  for the photometric data of a supernova at  $z = 0.325$ . The indices of the photometric data points are ordered by the band and by the epoch of observation within each band. There are 92 photometric points taken in each band, so the  $n$ 'th observation in the  $\alpha$ 'th band has index  $92\alpha + n$  where  $\alpha = 0$  for the  $g$ ,  $\alpha = 1$  for  $r$ ,  $\alpha = 2$  for  $i$ , and  $\alpha = 3$  for the  $z$  bands. The units and normalization of  $f$  are set by the SALT2  $x_0 = 1$  template in MKS units via Equations 1 and 4. The location of each point with respect to the light curve is identifiable through the middle plot  $\partial f/\partial x_0$ .

Table 3

$\mu$ - $z$  covariance and effective  $\mu$  uncertainties: Peak  $S/N = 50$ , four-day cadence

$z_{SN}$	$\sigma_{prior}(z) = \text{none}$		$\sigma_{prior}(z) = 0.01$		$\sigma_{prior}(z) = 10^{-3}$	
	$\mathbf{U}$	$\sigma_{\mu,eff}$	$\mathbf{U}$	$\sigma_{\mu,eff}$	$\mathbf{U}$	$\sigma_{\mu,eff}$
0.325	$\begin{pmatrix} 0.0011 & 1.9E-4 \\ 1.9E-4 & 1.2E-4 \end{pmatrix}$	0.097	$\begin{pmatrix} 9.3E-4 & 8.9E-5 \\ 8.9E-5 & 5.4E-5 \end{pmatrix}$	0.069	$\begin{pmatrix} 7.9E-4 & 1.6E-6 \\ 1.6E-6 & 9.9E-7 \end{pmatrix}$	0.029
0.731	$\begin{pmatrix} 0.0010 & 7.3E-5 \\ 7.3E-5 & 4.4E-5 \end{pmatrix}$	0.043	$\begin{pmatrix} 0.0010 & 5.0E-5 \\ 5.0E-5 & 3.0E-5 \end{pmatrix}$	0.040	$\begin{pmatrix} 9.3E-4 & 1.6E-6 \\ 1.6E-6 & 9.8E-7 \end{pmatrix}$	0.031
1.118	$\begin{pmatrix} 0.044 & 0.0048 \\ 0.0048 & 6.4E-4 \end{pmatrix}$	0.25	$\begin{pmatrix} 0.013 & 6.5E-4 \\ 6.5E-4 & 8.6E-5 \end{pmatrix}$	0.12	$\begin{pmatrix} 0.0079 & 7.5E-6 \\ 7.5E-6 & 1.0E-6 \end{pmatrix}$	0.089

There is no guarantee that SNe Ia can be better standardized than currently done by SALT2. However, the optimist may imagine that with enough data and refinement, the SALT2 model could eventually perfectly describe supernovae in at all wavelengths. Table 4 shows the improved results when no model dispersion (i.e. no contribution from Equation 8) is included in the error budget.

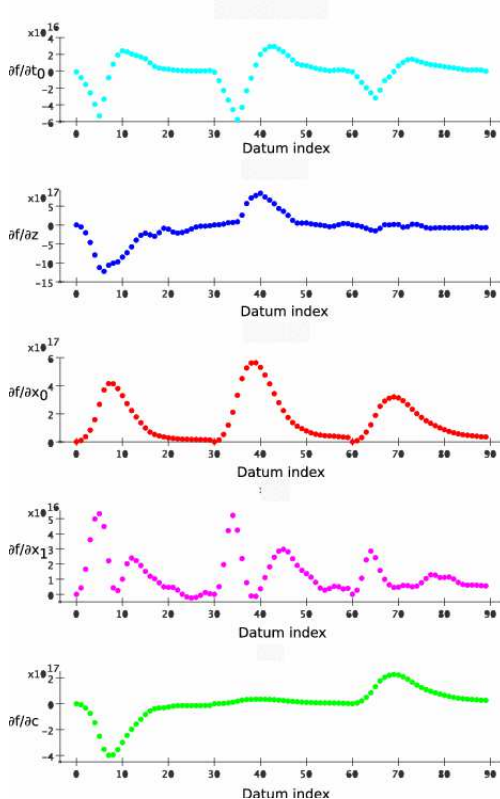


Fig. 2. The same as in Figure 1 for the 90 data points of a supernova at  $z = 0.731$ . The data correspond, from left to right, to observations in *riz*-bands.

Table 4

$\mu$ - $z$  covariance and effective  $\mu$  uncertainties: Peak  $S/N = 25$ , four-day cadence, no model residuals

$z_{SN}$	$\sigma_{prior}(z) = \text{none}$		$\sigma_{prior}(z) = 0.01$		$\sigma_{prior}(z) = 10^{-3}$	
	$\mathbf{U}$	$\sigma_{\mu,eff}$	$\mathbf{U}$	$\sigma_{\mu,eff}$	$\mathbf{U}$	$\sigma_{\mu,eff}$
0.325	$\begin{pmatrix} 6.7E-4 & 1.4E-4 \\ 1.4E-4 & 1.4E-4 \end{pmatrix}$	0.097	$\begin{pmatrix} 5.9E-4 & 5.9E-5 \\ 5.9E-5 & 5.9E-5 \end{pmatrix}$	0.065	$\begin{pmatrix} 5.3E-4 & 9.9E-7 \\ 9.9E-7 & 9.9E-7 \end{pmatrix}$	0.024
0.731	$\begin{pmatrix} 0.0016 & 1.6E-4 \\ 1.6E-4 & 5.1E-5 \end{pmatrix}$	0.055	$\begin{pmatrix} 0.0014 & 1.1E-4 \\ 1.1E-4 & 3.4E-5 \end{pmatrix}$	0.049	$\begin{pmatrix} 0.0011 & 3.1E-6 \\ 3.1E-6 & 9.8E-7 \end{pmatrix}$	0.033
1.11	$\begin{pmatrix} 0.068 & 0.0085 \\ 0.0085 & 0.0011 \end{pmatrix}$	0.32	$\begin{pmatrix} 0.0100 & 6.9E-4 \\ 6.9E-4 & 9.2E-5 \end{pmatrix}$	0.11	$\begin{pmatrix} 0.0049 & 7.5E-6 \\ 7.5E-6 & 1.0E-6 \end{pmatrix}$	0.070

All results presented in this paper are calculated for the case where observations are phased to begin on the date of explosion. In the case of  $S/N = 25$  and no redshift priors, results vary by  $< 1\%$  depending on the phase of observations with respect to the underlying light curve.

## 4 Discussion

There are several interesting features of our results that we discuss here in further detail.



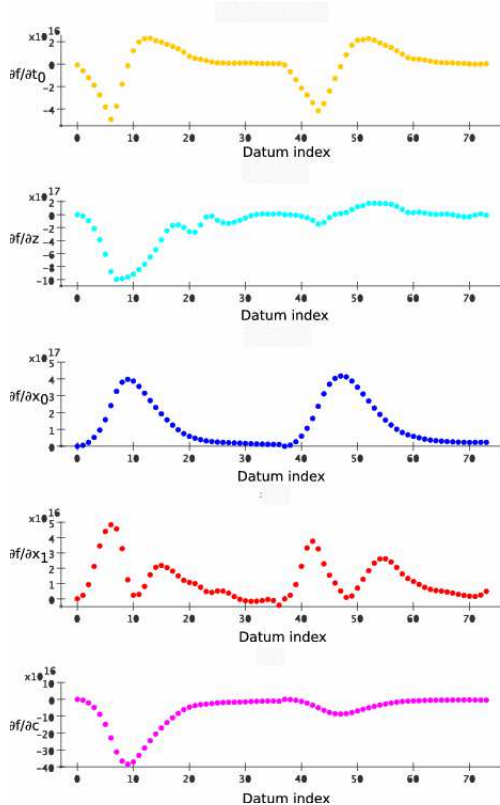


Fig. 3. The same as in Figure 1 for the 74 data points of a supernova at  $z = 1.118$ . The data correspond, from left to right, to observations in  $iz$ -bands.

Distance modulus and redshift measurements have significant positive correlation when there are no or weak redshift priors. The correlation is dominated by the contribution of  $\alpha \times (\mathbf{F}^{-1})_{x_1 z}$ . The positive  $(\mathbf{F}^{-1})_{x_1 z}$  is due to the supernova-frame  $U$ -band, where a strongly negative  $\partial f / \partial z$  arises from the band coverage over the transition between the UV-flux dropout to the bright  $B$  emission ubiquitous to SNe Ia. On the other hand, SALT2 predicts brighter UV flux for larger  $x_1$ . The coverage over Ca H&K wavelengths is therefore important for distinguishing supernova redshift and light-curve shape.

The effective distance modulus uncertainty is more sensitive to redshift uncertainties at low redshift. For example, in the case of no redshift prior,  $z = 0.325$  and  $S/N = 25$ , the large value of  $(d\mu_\gamma/dz)^2$  makes it such that  $\sigma_{\mu,eff}$  comes almost entirely from the  $(\frac{d\mu_\gamma}{dz})^2 U_{zz}$  term. The approximation derived in §A to get Equation 7 breaks down as  $\sigma_z d\mu_\gamma/dz$  gets close to or larger than  $\sigma_\mu$ , which is certainly the case at low redshifts. By  $z = 0.731$  the effective distance uncertainty is dominated by the  $U_{\mu\mu}$  contribution and our approximation holds. The  $d\mu_\gamma/dz$  term does give the effective distance modulus uncertainty a dependence on the cosmological parameters. A fit could proceed using the full  $\mu$ - $z$  covariance matrix, or iteratively with the values of the cosmological parameters updated using the fit from the preceding iteration.

Without redshift priors, the redshift uncertainties derived from supernova light curves range from 0.011–0.025 for the case of  $S/N = 25$ . Significant improvement in the cosmological utility of each supernova is possible with a comparable or better redshift prior. This is illustrated by the case of  $z = 1.118$  in Table 2. Without priors, the uncertainty in redshift is 0.025. When the redshift is constrained by a prior with 0.01 uncertainty, the resulting uncertainty in  $\mu$  drops precipitously from 0.21 to 0.11 mag<sup>2</sup>. Concern about redshift uncertainties are superfluous when spectrograph-quality redshifts  $\sigma_{prior}(z) = 10^{-3}$  are available. This shows why the propagation of redshift uncertainties is of little concern for experiments with spectroscopic redshifts.

It may seem odd that the covariance matrix  $\mathbf{U}$  gives smaller redshift uncertainties for the  $z = 0.731$  survey than for the  $z = 0.325$  survey, particularly since the latter has observations in four bands rather than three. By construction, the two surveys give the same  $S/N$  for their respective target redshift and both use comparable numbers of data points due to the extra time dilation experienced by the more distant object. Qualitative comparison of Figures 1 and 2 shows that  $\partial f/\partial z$  distinguishes  $z = 0.325$  from 0.731 supernovae. At the lower redshift,  $\partial f/\partial z$  and  $\partial f/\partial c$  have almost identical shapes whereas at  $z = 0.731$  they are visibly different in the third band, allowing for tighter constraints in  $z$  and  $c$ . The Fisher matrix calculation gives for  $z = 0.325$ :  $\sigma_z = 0.016$ ,  $\sigma_c = 0.028$  and  $\rho_{zc} = -0.72$  and for  $z = 0.731$ :  $\sigma_z = 0.0092$ ,  $\sigma_c = 0.021$  and  $\rho_{zc} = -0.41$ .

Differences in  $\partial f/\partial z$  between the two redshifts are due to differing contributions from

$$-\frac{1}{(1+z)^2} \int T_X(\lambda) \lambda \frac{\partial N_{\ln \lambda}}{\partial \lambda'}(p, \lambda') d \ln \lambda \quad (9)$$

where  $\lambda' = \lambda/(1+z)$ . This term reflects changes in the predicted observed light curves with redshifting of the supernova SED at fixed phase. (The phase dependent contribution to  $\partial f/\partial z$  strongly resembles  $\partial f/\partial t_0$ .) The different shapes and uneven  $\ln \lambda$ -spacing of the *griz*-bands give redshift-dependent observed supernova-frame wavelengths. Equation 9 is close to zero when the band covers the wavelength region with peak emission; at shorter wavelengths

<sup>2</sup> To give the reader the ability to explore other redshift priors, we provide the Fisher matrix for the supernova at  $z = 1.118$ :

$$\mathbf{F} = \begin{pmatrix} 41.979296 & 135.174711 & 26.890238 & -9.767684 & -11.22469 \\ 135.174711 & 9417.796467 & -2617.136017 & -204.29132 & 2893.102837 \\ 26.890238 & -2617.136017 & 4501.498662 & 262.329719 & -1834.985182 \\ -9.767684 & -204.29132 & 262.329719 & 39.340308 & -110.596575 \\ -11.22469 & 2893.102837 & -1834.985182 & -110.596575 & 1244.587705 \end{pmatrix}.$$

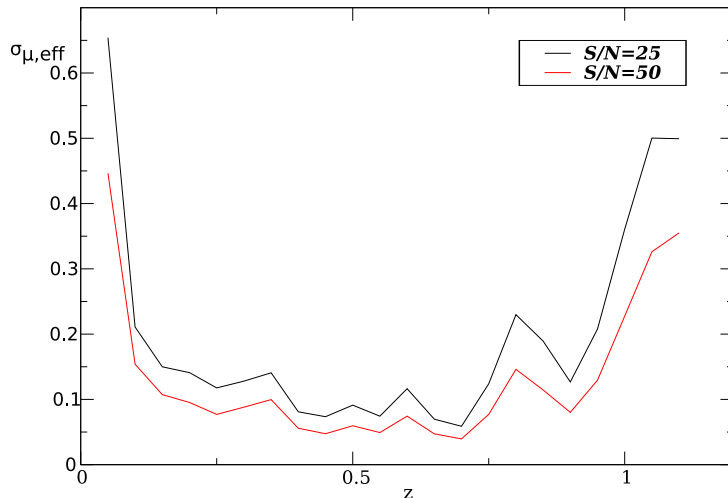


Fig. 4. Calculated  $\sigma_{\mu,eff}$  for a series of redshifts from  $z = 0.05 - 1.1$  in steps of 0.05, with  $S/N = 25$  and 50 photometry and no redshift prior. The low-frequency shape of the curve is due to the evolution of  $\frac{d\mu_\gamma}{dz}$  at low redshifts, and the decreasing amount of data and band coverage at high redshift. The high-frequency oscillatory behavior is due to differing coverage of the supernova SED by the observer bands and the resulting change in sensitivity to the light-curve parameters.

it is negative and at longer wavelengths it is positive. The pronounced peaks in the  $i$ -band  $\partial f/\partial z$  at  $z = 0.325$  and  $z = 0.731$  are attributable to their SN-frame wavelengths and the phase-dependent  $\frac{\partial N_{ln\Delta}}{\partial \lambda'}(p, \lambda')$ .

We calculate  $\sigma_{\mu,eff}$  for a series of redshifts from  $z = 0.05 - 1.1$  in steps of 0.05 for the cases of  $S/N = 25$  and 50 and no redshift prior, and show the results in Figure 4. Looking at the low-frequency behavior, at low redshift there is a dramatic decrease in  $\sigma_{\mu,eff}$  with increasing redshift as  $\frac{d\mu_\gamma}{dz}$  falls. At redshifts greater than  $z = 0.75$ ,  $\sigma_{\mu,eff}$  degrades as the number of usable data points and band coverage decreases. The high-frequency oscillatory behavior is due to differing coverage of the supernova SED by the observer bands and the resulting change in sensitivity to the light-curve parameters.

Comparison of Tables 2 and 4 indicates that photometry uncertainty in the  $S/N = 25$  scenario dominates over the uncertainty from the SALT2 light-curve templates. The covariance matrices for the case of no redshift prior differ by a factor of two between  $S/N = 25$  and  $S/N = 50$ , rather than the factor of four expected if there were no SALT2 uncertainties.

Selecting cadences of two, four, and eight days while keeping the peak signal-to-noise proportional to the square root of the cadence gives the same results within the second significant digit. Degradation is expected at higher cadences as supernova phases with leverage (large  $\partial f/\partial \mathbf{p}$ ) can be missed.

Extending the observer bands to include the  $Y$ -band can help significantly for objects at high redshift. For a  $z = 1.118$  supernova with  $S/N = 25$  at peak,  $\sigma_{\mu,eff}$  improves from 0.39 to 0.11 mag.

For the cases in this paper where  $\sigma_z > 0.01$ , we expect that a full Monte-Carlo-based fit would deviate from the Fisher estimate by something in the order of 10-20%; the broad wiggles in the supernova spectrum produce non-linear effects over this large redshift range.

## 5 Conclusions

In assessing whether a photometric survey produces adequate  $\mu$ - $z$  uncertainty, we set as a target achieving a  $\sigma_{\mu,eff}$  comparable to the intrinsic SN Ia magnitude dispersion,  $\sim 0.15$  mag. At this point, it is more advantageous to spend time observing more supernovae rather than improving the statistical precision of each individual object.

If relying on photometric information only, the observer can tune the depth of the survey to obtain the desired distance uncertainties. Measurements that give better than  $S/N = 50$  at peak brightness for an average  $x_1 = 0$ ,  $c = 0$  supernova in each band with a four-day observing cadence would be necessary to meet the target  $\sigma_{\mu,eff}$  out to  $z = 1.0$ . Survey changes that hold fixed  $(S/N)/\text{cadence}^2$  have almost no effect on  $\mu$ - $z$  uncertainty for the finely sampled light curves considered in this paper.

Improvements in photometric quality give declining yields when photometric uncertainties are smaller than those of the SN model. For our simulated data, SN model uncertainties begin to dominate between data qualities corresponding to our  $S/N = 25$  and  $S/N = 50$  surveys. Work on supernova modeling is ongoing and improvements are expected as data with better wavelength and temporal coverage are included in template building.

A judicious selection of observer bands and/or targeting of “magic” redshifts can give data with stronger leverage in minimizing the  $\mu$ - $z$  covariance matrix, as seen in Figure 4. These occur when there are strong distinctive light-curve gradients with respect to the redshift of the spectra, allowing the breaking of the degeneracy between redshift and other parameters.

Shallower surveys can use the subset of supernovae with redshift prior uncertainties of 0.01 or better. We expect that the patient or well-equipped observer can obtain spectroscopic redshifts of supernovae discovered out to  $z = 0.325$ . Complete spectra for an unbiased sample of supernova hosts at higher redshifts will be more of a challenge; for these, photometric redshifts can be used. Photometric redshift uncertainties of  $\sigma_{\Delta z/(1+z)} = 0.029$  for a galaxy subsample have been obtained with the CFHT filter set [15] and better performance can be obtained with the addition of a redder filter. A broader and non-Gaussian dispersion is expected, however, for the diverse population of supernova host galaxies.

In this paper, we do not consider biases in the SALT2 model. Biases in the distance and redshift determination leave irreducible uncertainties that impact cosmological parameter measurements. The size of the training set necessary for the SALT2 model construction and in testing its performance is subject for further study.

As supernova cosmologists concentrate on reducing the systematic uncertainties in using SNe Ia as distance indicators, focus is being placed on using light curves to distinguish variation in observed colors that are intrinsic to supernovae against those due to dust, and to determine the extinction properties of the host-galaxy dust itself. Other intrinsic supernova parameters may be encoded in the light curves. In addition, we have not considered the impact of assigning the light-curve fitter the additional responsibility of determining supernova type. Constructing a model for such a generalized fitter is difficult given the heterogeneity of core-collapse supernovae and the dearth of Ibc light curves, although Bayesian methods have been applied towards this problem [5,7]. The formalism presented in this paper can be applied to future sophisticated light-curve models with an expanded parameter set. With photometric information diverted towards the measurement of additional supernova features, the uncertainties in  $\mu$  and  $z$  can only degrade compared to the 3-parameter SALT2 model.

## Acknowledgements

We acknowledge helpful discussions with Julien Guy, Eric Linder, Lifan Wang, and Yun Wang. Thanks also to the Aspen Center for Physics where the idea for this paper and much of the work took place. We thank the referee for constructive comments. This work has been supported in part by the Director, Office of Science, Department of Energy under grant DE-AC02-05CH11231.

## A Joint Probability Density Function for Distance Modulus and Redshift

When attempting to determine the cosmological parameters using the information contained in the distance moduli and redshifts of a set of SNe Ia, the joint probability density function (pdf)  $p(\mu^o, z^o|\vec{\theta})$  for the distance modulus ( $\mu$ ) and redshift ( $z$ ) of each supernova is needed. Here, the superindex  $^o$  denotes observed quantities, while  $\vec{\theta}$  stands for the cosmological, and possibly nuisance, parameters. The pdf is the probability density for observing a  $(\mu^o, z^o)$  pair given  $\vec{\theta}$ . It can be computed as

$$p(\mu^o, z^o|\vec{\theta}) = \int d\mu^t \int dz^t p(\mu^o, z^o|\mu^t, z^t) p(\mu^t, z^t|\vec{\theta}), \quad (\text{A.1})$$

where we integrate over all possible true values for  $\mu$  and  $z$ . The first pdf in the right-hand side of (A.1) is just a two-dimensional resolution Gaussian relating the observed and the true values of  $\mu$  and  $z$ . The second pdf can be written as

$$\begin{aligned} p(\mu^t, z^t|\vec{\theta}) &= p(\mu^t|z^t, \vec{\theta}) p(z^t|\vec{\theta}) \\ &= \delta(\mu^t - \bar{\mu}(z^t, \vec{\theta})) p(z^t) \\ &\propto \delta(\mu^t - \bar{\mu}(z^t, \vec{\theta})), \end{aligned} \quad (\text{A.2})$$

where  $\bar{\mu}(z^t, \vec{\theta})$  is the distance modulus that results from applying the Hubble relationship to the true redshift, considering the values of the parameters  $\vec{\theta}$ . In writing the last proportionality relationship we have taken into account that  $p(z^t|\vec{\theta})$  does not depend on  $\vec{\theta}$  and, therefore, can be safely neglected in the following. Therefore, we have

$$\begin{aligned} p(\mu^o, z^o|\vec{\theta}) &\propto \int_{-\infty}^{+\infty} d\mu \int_{-\infty}^{+\infty} dz \exp \left[ -\frac{1}{2} (\mu^o - \mu, z^o - z)^T \mathbf{U}^{-1} (\mu^o - \mu, z^o - z) \right] \delta(\mu - \bar{\mu}(z, \vec{\theta})) \\ &= \int_{-\infty}^{+\infty} dz \exp \left[ -\frac{1}{2} (\mu^o - \bar{\mu}(z, \vec{\theta}), z^o - z)^T \mathbf{U}^{-1} (\mu^o - \bar{\mu}(z, \vec{\theta}), z^o - z) \right]. \end{aligned} \quad (\text{A.3})$$

In the last equation we have dropped the  $^t$  superindices for simplicity, and we have used the delta function to perform the integral over  $\mu$ .  $\mathbf{U}$  is the  $2 \times 2$  covariance matrix for the observation of  $\mu^o$  and  $z^o$ . In order to simplify the calculations that follow, we will assume for the moment that  $\mathbf{U}$  is a diagonal matrix with elements  $\sigma_\mu^2, \sigma_z^2$ . In this case, Equation (A.3) simplifies to:

$$p(\mu^o, z^o|\vec{\theta}) \propto \int_{-\infty}^{+\infty} dz \exp \left[ -\frac{1}{2} \left( \frac{\mu^o - \bar{\mu}(z, \vec{\theta})}{\sigma_\mu} \right)^2 \right] \exp \left[ -\frac{1}{2} \left( \frac{z^o - z}{\sigma_z} \right)^2 \right]. \quad (\text{A.4})$$

Although the integral extends to all possible values of  $z$ , it is clear from the second exponential that only values of  $z$  sufficiently close to  $z^o$  will actually contribute. Let us, then, expand  $\bar{\mu}(z, \vec{\theta})$  about  $z^o$  as

$$\bar{\mu}(z, \vec{\theta}) \simeq \bar{\mu}(z^o, \vec{\theta}) + \left. \frac{d\mu}{dz} \right|_{z^o} (z - z^o). \quad (\text{A.5})$$

Introducing Equation (A.5) into Equation (A.4) leads to

$$p(\mu^o, z^o | \vec{\theta}) \sim \int_{-\infty}^{+\infty} dz \exp \left[ -\frac{1}{2\sigma_\mu^2} \left( \mu^o - \bar{\mu}(z^o, \vec{\theta}) - \left. \frac{d\mu}{dz} \right|_{z^o} (z - z^o) \right)^2 \right] \exp \left[ -\frac{1}{2} \left( \frac{z^o - z}{\sigma_z} \right)^2 \right], \quad (\text{A.6})$$

which is just a Gaussian integral in  $z$ . It can be easily computed to give:

$$p(\mu^o, z^o | \vec{\theta}) \sim \exp \left[ -\frac{1}{2} \left( \frac{\mu^o - \bar{\mu}(z^o, \vec{\theta})}{\sigma} \right)^2 \right]. \quad (\text{A.7})$$

So finally the desired pdf is a Gaussian distribution centered at the expected distance modulus for the measured redshift and with variance  $\sigma^2 = \sigma_\mu^2 + \left( \frac{d\mu}{dz} \sigma_z \right)^2$ , where the derivative is to be taken at  $z = z^o$ . If the covariance matrix  $\mathbf{U}$  between  $\mu^o$  and  $z^o$  is non-diagonal, the resulting pdf is still a Gaussian with the same mean but with variance  $\sigma^2 = \sigma_\mu^2 + \left( \frac{d\mu}{dz} \sigma_z \right)^2 + 2\rho \frac{d\mu}{dz} \sigma_\mu \sigma_z$ , where  $\rho$  is the correlation coefficient between  $\mu^o$  and  $z^o$ .

## References

- [1] W. L. Freedman, et al., ApJ 553 (2001) 47–72.
- [2] A. G. Riess, et al., AJ 116 (1998) 1009.
- [3] S. Perlmutter, et al., ApJ 517 (1999) 565–586.
- [4] G. Aldering, A. G. Kim, M. Kowalski, E. V. Linder, S. Perlmutter, APh 27 (2007) 213–225.
- [5] B. J. Barris, J. L. Tonry, ApJ 613 (2004) L21–L24.
- [6] B. D. Johnson, A. P. S. Crotts, AJ 132 (2006) 756–768.
- [7] N. V. Kuznetsova, B. M. Connolly, ApJ 659 (2007) 530–540.
- [8] M. Sullivan, et al., AJ 131 (2006) 960–972.
- [9] Y. Wang, ApJ 654 (2007) L123–L125.
- [10] D. Huterer, A. Kim, L. M. Krauss, T. Broderick, ApJ 615 (2004) 595–602.

- [11] J. Guy, et al., *A&A* 466 (2007) 11–21.
- [12] P. Nugent, A. Kim, S. Perlmutter, *PASP* 114 (2002) 803–819.
- [13] P. Astier, et al., *A&A* 447 (2006) 31–48.
- [14] M. Tegmark, A. Taylor, A. Heavens, *ApJ* 480 (1997) 22.
- [15] O. Ilbert, et al., *A&A* 457 (2006) 841–856.